

Effect of Pressure on Valence and Structural Properties of YbFe_2Ge_2 Heavy Fermion Compound—A Combined Inelastic X-ray Spectroscopy, X-ray Diffraction, and Theoretical Investigation

Ravhi S. Kumar,^{*,†} Axel Svane,[§] Ganapathy Vaitheeswaran,^{||} Venkatakrishnan Kanchana,[⊥] Daniel Antonio,[†] Andrew L. Cornelius,[†] Eric D. Bauer,[‡] Yuming Xiao,[#] and Paul Chow[#]

[†]Department of Physics and Astronomy and HiPSEC, University of Nevada Las Vegas, Las Vegas, Nevada 89154, United States

[‡]Los Alamos National Laboratory, P.O. Box 1663, MS K764, Los Alamos, New Mexico 87545, United States

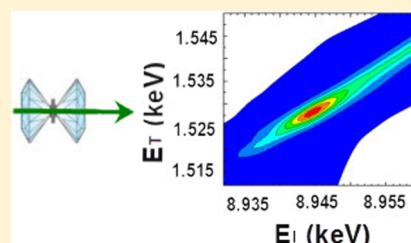
[§]Department of Physics and Astronomy, Aarhus University, DK-8000 Aarhus C, Denmark

^{||}Advanced Centre of Research in High Energy Materials (ACRHEM), University of Hyderabad, Gachibowli, Hyderabad – 500 046, Telangana, India

[⊥]Department of Physics, Indian Institute of Technology Hyderabad, Ordnance Factory Estate, Yeddumailaram – 502 205, Telangana, India

[#]HPCAT, Carnegie Institution of Washington and Advance Photon Source, Argonne National Laboratory, Argonne, Illinois 60439, United States

ABSTRACT: The crystal structure and the Yb valence of the YbFe_2Ge_2 heavy fermion compound was measured at room temperature and under high pressures using high-pressure powder X-ray diffraction and X-ray absorption spectroscopy via both partial fluorescence yield and resonant inelastic X-ray emission techniques. The measurements are complemented by first-principles density functional theoretical calculations using the self-interaction corrected local spin density approximation investigating in particular the magnetic structure and the Yb valence. While the ThCr_2Si_2 -type tetragonal ($I4/mmm$) structure is stable up to 53 GPa, the X-ray emission results show an increase of the Yb valence from $\nu = 2.72(2)$ at ambient pressure to $\nu = 2.93(3)$ at ~ 9 GPa, where at low temperature a pressure-induced quantum critical state was reported.



1. INTRODUCTION

Solids containing elements from the rare earth series show interesting and unusual behavior associated with the versatility of the manifold of 4f electrons, including Kondo screening, heavy fermion, and intermediate valence behavior, sometimes with competing magnetism and superconductivity.^{1–5} Prominent examples are CeT_2M_2 and YbT_2M_2 (where T denotes a transition metal ion and M denotes Si or Ge),¹ which may exhibit transitions from magnetic to heavy-fermion ground states as a function of pressure or magnetic field. If the magnetism is suppressed to $T = 0$ K by the application of such an external parameter, a quantum critical point appears (QCP), in which strong quantum fluctuations give rise to unusual, or non-Fermi, liquid temperature dependencies of the physical properties. Several competing low-energy scales are set by the rare earth valence fluctuation, the f to non-f hybridization, the crystal fields, the exchange interactions, and the spin-fluctuations, all of which contribute to rich low-temperature phase diagrams.^{1–5}

YbFe_2Ge_2 crystallizes in the body-centered tetragonal ThCr_2Si_2 structure, which is common to many compounds in the rare earth “122 class”.^{6,7} YbFe_2Ge_2 has been identified as a moderate heavy fermion system at the border between the Kondo and the intermediate valence regime.⁸ The susceptibility

and specific heat measurements show a nonmagnetic Fermi liquid state. The structural parameters, the variable Yb valence, and the delicate complex interactions between the magnetic moments of the constituent elements lead to quantum criticality, and with pressure the Fermi liquid state is driven to a magnetically ordered state at the QCP at a critical pressure of 9 GPa. In contrast to the Ce-122 compounds,⁹ the Neel temperature increases as a function of pressure, and antiferromagnetic ordering develops above the QCP.^{8,10} Electronic structure calculations of the non-f YFe_2Ge_2 homologue have shown that the band structure and Fermi surfaces are three-dimensional with Stoner-type magnetism associated with the Fe layers. The most favorable structure consists of ferromagnetically ordered Fe layers, which are antiferromagnetically coupled along the c-axis.^{11,12} Experimentally, fluctuating local Fe moments have been identified from high-temperature susceptibility measurements.¹³ The situation is similar for LuFe_2Ge_2 .^{14,15} Even though the resistivity measurements on YbFe_2Ge_2 reported earlier did not reveal any superconducting signature,¹⁰ recently YFe_2Ge_2 is reported to show Fermi liquid breakdown, which may be connected to

Received: July 9, 2015

Published: October 19, 2015

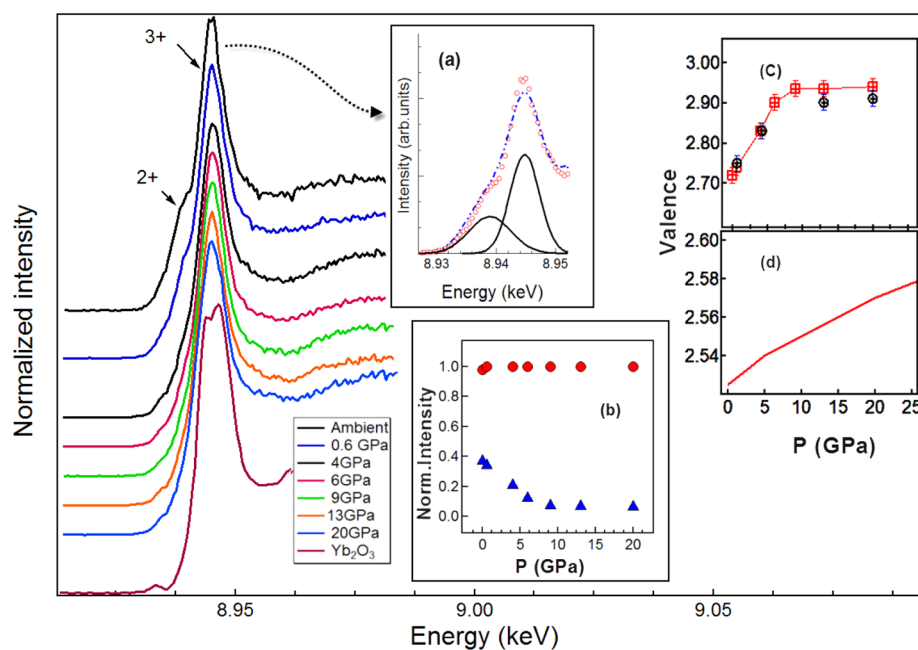


Figure 1. X-ray absorption spectra collected in the PFY mode at various pressures. The arrows indicate the contributions from the Yb^{2+} and Yb^{3+} components. (a) Fitting of the divalent and trivalent components for the ambient spectrum is shown as an example. (b) The change of intensity of divalent (\blacktriangle) and trivalent (\square) contributions as a function of pressure. (c) Variation of Yb valence as a function of pressure observed in the experiments. The square symbols indicate the valence obtained from PFY measurements, and the circles represent the data from RXES measurements. (d) Valence estimated from the theoretical simulations.

the QCP.¹⁶ Resistivity and direct-current diamagnetic screening suggest that YFe_2Ge_2 superconducts below 1.8 K in the vicinity of the QCP.¹⁶ To explore the origin of QCP, the interplay between crystal structure and valence as a function of pressure is important. We show that the Yb effective valence at room temperature is sensitive to pressure, with a value of $\nu = 2.72(2)$ at ambient pressure, and approaches near trivalency, $\nu = 2.93(3)$ at pressures above 9 GPa. However, the pressure–volume (PV) relation shows no peculiarities associated with the pressure-induced valence transition, which is in contrast to the case of YbMn_2Ge_2 , where a similar—though more abrupt—valence transition is seen in association with a distinct anomaly in the PV relation.¹⁷

The present paper investigates the impact of the QCP, which has been observed in YbFe_2Ge_2 at low temperatures,^{8,10} on the crystal structure and effective Yb valence at room temperature as pressure is varied across the critical pressure (p_c) of 9 GPa. A combination of high-pressure X-ray diffraction (HPXRD), resonant X-ray emission spectroscopy (RXES), and X-ray absorption spectroscopy (XAS) in the partial fluorescence yield (PFY) mode are used, with pressures up to 53 GPa for the structural measurements and 20 GPa for the valence studies, respectively. In PFY-XAS scans the intensity of the emitted Yb $L\alpha$ fluorescence was measured while scanning the energy of the primary beam. RXES has been applied to investigate a variety of Yb intermetallic and other heavy fermion compounds.^{17–20} RXES enables the valence to be determined with incident photon energies being selected to enhance signals from different valence states. To further analyze the experiments electronic structure calculations have been performed for YbFe_2Ge_2 using the self-interaction corrected local spin-density (SIC-LSD) method.^{21,22} This ab initio electronic structure method allows studying the pure divalent and trivalent states of Yb as well as an approximate model of the intermediate valence state. The ground state is then determined by use of the total

energy. Previous applications of the SIC-LSD method for determining the Yb valence in intermetallic compounds may be found in the literature.^{23–27}

2. METHODOLOGY

2.1. Experiments. The YbFe_2Ge_2 polycrystalline sample was prepared by induction melting the appropriate starting elements, which were in a graphite crucible in the ratio of Yb/Fe/Ge = 1.05:2:2 in an Ar-inert atmosphere, and was heated to $\sim 1100 \pm 50$ C determined using an optical pyrometer and rapidly quenched. The sample was subsequently characterized by powder XRD, which showed a single phase formation for the sample with the ThCr_2Si_2 -type tetragonal crystal structure (space group no. 139, $I4/mmm$). The finely ground powdered sample was introduced with a few ruby grains and Si fluid in a 150 μm diameter hole of a Be gasket and loaded to a panoramic-type diamond anvil cell for X-ray emission experiments. High-pressure X-ray emission experiments were performed at Sector 16 ID-D of the Advanced Photon Source by focusing the incident X-ray beam to dimensions of 20 $\mu\text{m} \times 50 \mu\text{m}$ at the Yb L_3 absorption edge (8.944 keV) with an energy resolution of 1 eV. Both PFY and RXES spectra were collected up to 20 GPa. The pressure in the diamond cell was measured using the ruby fluorescence technique.

For the HPXRD experiments a symmetric-type diamond anvil cell was used. A dense piece cut from a pellet made from the fine powdered sample and a few ruby grains were introduced into a 135 μm hole of a rhenium gasket preindented to 50 μm . A Silicone fluid pressure medium was used, and the HPXRD experiments were performed up to 53 GPa at Sector 16 ID-B of the Advanced Photon Source in the angle dispersive geometry. The pressure in the diamond cell was determined using the ruby fluorescence technique as mentioned earlier. Diffraction images were collected using a MAR-345 imaging plate with an incident wavelength of $\lambda = 0.4216$ Å and integrated using the Fit2D software.²⁸ The sample-to-detector distance was calibrated using a CeO_2 sample spectrum. The integrated diffraction patterns were further analyzed using the JADE and Rietveld (RIETICA) packages.²⁹

2.2. Theoretical Calculations. The theoretical description of fluctuating valence systems is notoriously difficult using conventional

LDA methods.³⁰ In the present work the electronic structure of YbFe_2Ge_2 was calculated with the self-interaction corrected (SIC) local spin density (LSD) method,^{21,22,31} similar to previous work on YbMn_2Ge_2 .²⁰ In the SIC-LSD method the effective one-electron potential includes a correction for the spurious interaction of individual electrons with themselves.²² This term favors the formation of spatially localized states as compared to extended Bloch waves and leads to a scheme for the calculation of cohesive properties of rare-earth compounds.^{22,31}

In applications to Yb compounds^{25,26} the SIC-LSD method may describe the pure trivalent and divalent configurations of Yb as well as an intermediate valence state, the latter through an approximate ansatz for the many-electron wave function. The computed total energy for each of these three cases determines the ground-state configuration. The divalent state is realized by applying the self-interaction correction to all 14 f-electrons of Yb, while the pure trivalent state is realized by applying the self-interaction to 13 f-electrons and prohibiting the 14th f-electron from being occupied by projecting it out of the band subspace.

In the approximate model of the intermediate valence state, 13 f-electrons are localized on each Yb ion by the self-interaction correction, while the 14th f-electron is allowed to hybridize and form a band that is pinned at the Fermi level. The degree of filling of this band determines the effective Yb valence. If the filling is x , it implies that the wave function may be decomposed into a Yb f^{14} component with weight x and an Yb f^{13} component with weight $1 - x$. Hence, this band filling is directly comparable to the effective valence as derived from an experimental spectrum, which involves a superposition of components from either of the two Yb configurations, f^{13} and f^{14} , as is the case for the PFY and RXES experiments. The method has previously been applied to study the behavior of YbAl_3 ²⁰ and YbMn_2Ge_2 ¹⁷ under pressure, as well as to the pressure-induced isostructural phase transitions in the Yb chalcogenides.²⁷ The present implementation of the SIC-LCD method includes spin-orbit coupling and uses the linear muffin-tin orbital method³² in the tight-binding formulation.³³ Further technical details of the implementation are explained by A. Svane.²²

3. RESULTS AND DISCUSSION

3.1. Effect of Pressure on Yb Valence. The PFY spectra for selected pressures up to 20 GPa are shown in Figure 1a. The divalent ($E = 8.938$ keV) and trivalent ($E = 8.945$ keV) contributions may easily be differentiated in the PFY spectrum collected at ambient pressure. The intensities of the divalent and trivalent peaks are estimated by fitting each PFY spectrum using multipeak fitting with Lorentzian function. The intensity contributions are then used to estimate the valence of Yb at each pressure. Energy resolution of the incoming beam is 2.2 eV. The spectrometer energy resolution is 0.7 eV. The core-hole lifetime broadening from the Yb L_3 edge is ~ 4.6 eV. The total broadening is ~ 5.2 eV.

The PFY spectrum collected for a Yb_2O_3 sample showing the trivalent valence contribution for Yb is also depicted for comparison. When the pressure was increased to 0.6 GPa, the intensity of the 2+ peak starts to decrease (Figure 1b). A rapid reduction in the 2+ intensity is observed with further increase in pressure above 4 GPa. The average Yb valence obtained from both PFY and RXES experiments is plotted as a function of pressure (Figure 1c). Valence obtained using theoretical simulation is shown in Figure 1d.

The RIXS spectra obtained for two different pressures (0.6 and 20 GPa) are shown in Figure 2. Because of the strong $L\alpha$ fluorescence accompanying the RIXS spectra, the analysis is complicated. We fitted the fluorescence in the background as described previously;¹⁹ however, there exists a slight discrepancy between the estimated valence from PFY and RXES. The

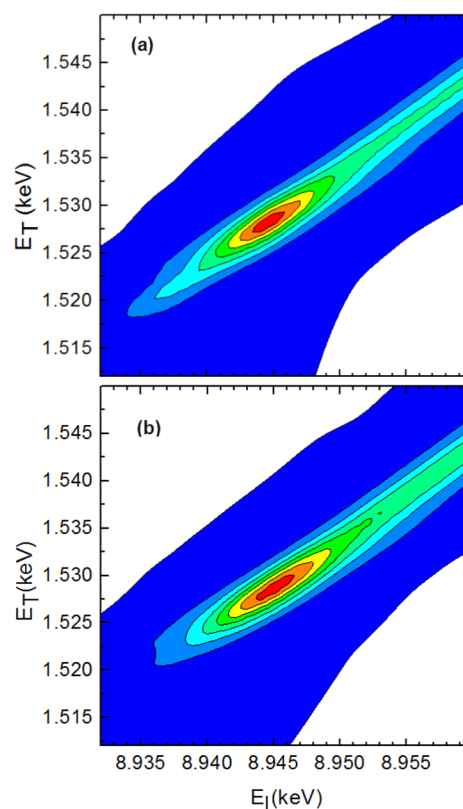


Figure 2. RIXS spectra collected at two different pressures 0.6 GPa (upper) and 20 GPa (lower). E_i represents the incident energy, and E_T is the transmitted energy.

plot shows an increase in the Yb effective valence with pressure from $\nu = 2.72(2)$ at ambient pressure to a nearly trivalent state $\nu = 2.93(3)$ above 9 GPa. The similar pressure-induced valence transition seen in YbMn_2Ge_2 ²⁰ is more abrupt, starting from $\nu = 2.42$ at ambient pressure, increasing steeply to $\nu = 2.75$ at $p = 1.35$ GPa and then evolving more steadily toward $\nu = 2.95$ above 15 GPa. Thus, if the YbMn_2Ge_2 transition is considered a two-step process (a fast ($d\nu/dp \approx 0.25$ GPa^{-1}) and a slow ($d\nu/dp \approx 0.014$ GPa^{-1}) valence transition, it appears as if YbFe_2Ge_2 only exhibits the second, slower, valence transition with a valence transition rate of $d\nu/dp \approx 0.022$ GPa^{-1}).

To investigate the change in Yb valence theoretically, the total energy of YbFe_2Ge_2 was calculated as a function of volume (Figure 3) assuming a ferromagnetic arrangement of localized Yb moments and considering divalent, trivalent, or intermediate valent Yb configurations. The Fe atoms are found to develop itinerant moments of the same direction as the Yb magnetic moments, which are dominated by the orbital contribution (see Subsection 3.3). The experimental ambient values of the c/a lattice parameter ratio and the Ge internal coordinate were fixed during the volume variation. The lowest energy is found for the mixed-valent state, at the volume $V_{0t} = 77.3$ \AA^3 . This is 4.5% below the experimental equilibrium volume of $V_{0e} = 80.9$ \AA^3 and reflects the usual overbinding in the LSD approximation.

The effective Yb valence in the mixed valence state is depicted in the inset of Figure 1b as a function of pressure. The trend is a linearly increasing behavior with pressure, with an effective valence of $\nu = 2.54$ (2.51) at the theoretical (experimental) equilibrium volume. This should be compared to the Yb effective valence of $\nu = 2.72(3)$ determined

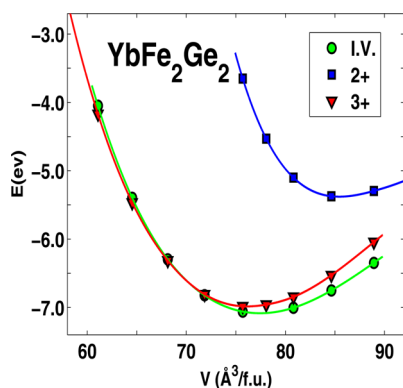


Figure 3. Total energy (in electronvolts per formula unit) vs specific volume (in cubic angstroms per formula unit) for YbFe_2Ge_2 for three different valence configurations of Yb (I.V. represents intermediate valence).

experimentally. The slope of the curve of the calculated effective valence is rather low, $dv/dp = 1.9 \times 10^{-3} \text{ GPa}^{-1}$, in contrast to the rapid change observed in the experiments, which is roughly 10 times higher. From Figure 2 it is seen that the pure divalent and trivalent states of Yb lead to higher total energies at the volume corresponding to the minimum energy of the mixed valence calculation, but upon compression, the trivalent and mixed-valent states rapidly approach each other and are indistinguishable for volumes lower than 72 \AA^3 . This implies that at this volume, corresponding to a compression of $V/V_{0t} = 0.93$ ($V/V_{0e} = 0.89$), the Yb valence tends to transform into the trivalent state. It is likely that the electronic structure of the Yb ion in YbFe_2Ge_2 is extremely sensitive to temperature and that the direct quantitative comparison between the present experiments (conducted at $T = 300 \text{ K}$) and theory (valid for $T = 0$) is not possible.

3.2. Crystal Structure at High Pressure and Equation of State. The PV data at room temperature shown in Figure 4 for YbFe_2Ge_2 were analyzed using a second-order Birch–Murnaghan equation of state (EOS).³⁴ The fitted EOS, shown as a solid line, matches well the experimental data. The bulk modulus (B_0) and its pressure derivative (B_0') at ambient pressure obtained for YbFe_2Ge_2 are $B_0 = 161(2) \text{ GPa}$ and $B_0' = 3.9(2)$. The corresponding results from the SIC-LSD theory are $B_0 = 183 \text{ GPa}$ and $B_0' = 5.1$ in reasonable agreement. In the $I4/mmm$ tetragonal symmetry Yb atoms are located in the 2a (0, 0, 0) positions, Fe atoms are at 4d (0, 0.5, 0.25) positions, and Ge atoms are at 4e (0, 0, z) positions.³⁵ The internal coordinate z for Ge is 0.4121(4) at the lowest pressure 1.5 GPa. This is comparable to that of YbMn_2Ge_2 ,¹⁷ for which $z = 0.3924$. The Rietveld refinement for the diffraction profile obtained at 8.5 GPa (near the critical pressure for the QCP) is also shown in Figure 3. The z parameter of Ge at this pressure is found to be $z = 0.3933(6)$. Upon compression only marginal changes are seen in the z-coordinate since the tetragonal symmetry is preserved up to 50 GPa. Also, no structural anomalies were observed throughout this pressure range. The fit to the EOS data for YbFe_2Ge_2 showed a higher bulk modulus in comparison with YbMn_2Ge_2 , for which $B_0 = 86 \text{ GPa}$ is found for the regular part of the compression curve above 1.3 GPa.¹⁷ The higher bulk modulus observed for the Fe compound compared to the Mn compound is similar to the trend observed for the elemental solids; that is, bulk Mn is considerably softer than bulk Fe, and shows that a significant part of the bonding in

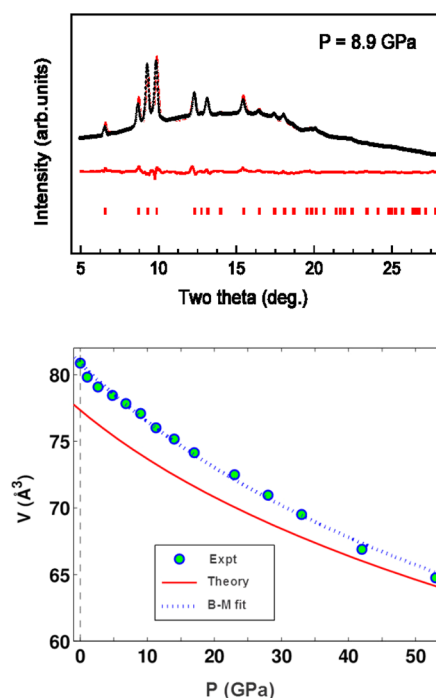


Figure 4. Pressure-dependent structural data for YbFe_2Ge_2 . (upper) The Rietveld refinement at 8.9 GPa for the tetragonal phase. The difference line and phase markers are shown below (in red). (lower) The PV relation, where the experimental points are marked with (blue) circles with the fitted Birch–Murnaghan PV curve given as a dashed line. The full (red) line represents the PV relation as calculated with the SIC-LSD theory.

the YbT_2Ge_2 compounds stems from the transition metal atoms occupying the 4d sites of the ThCr_2Si_2 structure. Bulk modulus values closer to that of YbFe_2Ge_2 are reported for YbIr_2Si_2 (190 GPa)³⁶ and YbRh_2Si_2 (187 GPa).³⁷

On the basis of our high-pressure XES and XRD results we could further comment on the QCP in YbFe_2Ge_2 . According to Miyake et al.,³⁸ for valence-driven QCP, one would expect a notable volume collapse around the P_c in the PV plot with an abrupt increase in valence. The PV data at $T = 300 \text{ K}$ show a gradual decrease of volume and an increase in Yb valence under pressure. Even though the volume decreases rapidly as a function of pressure below the QCP, there are no anomalies in the compressibility. The absence of any first-order transition around the critical pressure (9 GPa) suggests that the QCP in YbFe_2Ge_2 may be of the conventional Hertz–Millis-type scenario.³ However, since our experiments are only performed at $T = 300 \text{ K}$, further experiments at low temperature are necessary to explore the nature of the quantum criticality in this system.

3.3. Magnetic Structure and Density of States—Theoretical Analyses. In Figure 5 the calculated volume variation of the Fe and Yb magnetic moments are shown. The Fe spin moments align antiparallel to the Yb spin moments. However, the Yb orbital moment is also antiparallel to the Yb spin moment and numerically larger, so the total magnetic moments of Fe and Yb are parallel. The moments are projected along the crystalline c-axis, and the spin moments include a g-factor of 2. The Fe spin moments are rapidly quenched under compression. The orbital moment of Fe is not shown, but it is small, $\sim 0.02 \mu_B$ at V_{exp} and decreasing under compression.

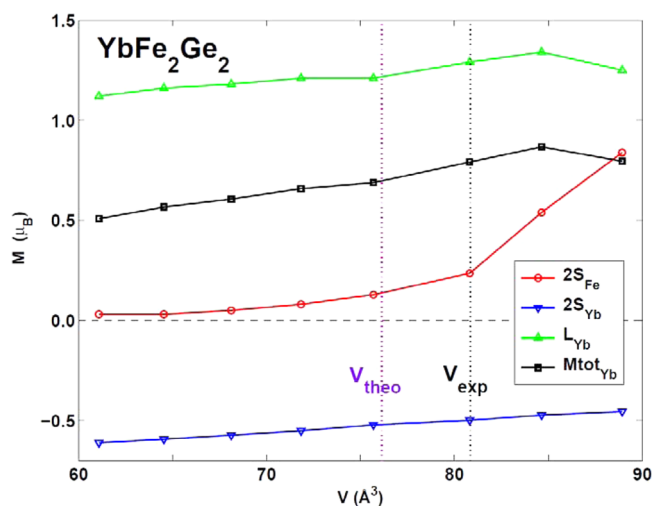


Figure 5. Calculated volume variation of the Fe spin moments (red \circ), Yb spin moments (blue ∇), orbital moments (green \triangle), and total moments (\square). The atomic spin moments are opposite in direction, but the total moments are aligned. The Fe moment shows the most distinct volume dependence. The theoretical and experimental equilibrium volumes are marked by vertical dotted lines.

At ambient conditions the magnetic phase diagram is discussed previously.⁸ To the best of our knowledge no experimental investigations on the pressure dependence of the magnetic properties of YbFe_2Ge_2 have been reported. The electronic density of states is presented in Figure 6.

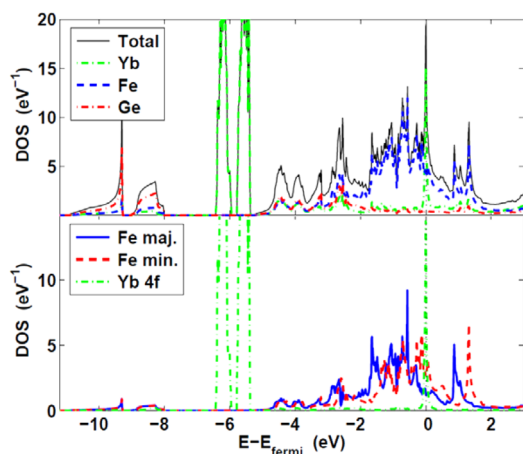


Figure 6. The density of electronic states for YbFe_2Ge_2 . The Fermi level is set to zero. (upper) The partial contributions from Yb, Fe, and Ge atoms, marked in green, blue, and red, respectively. (lower) The partial contributions from Fe majority and minority spins and from the Yb f states, in blue, red and green, respectively.

The calculated electronic density of states of YbFe_2Ge_2 is displayed in Figure 6 for the case of the intermediate valence scenario. The 13 localized Yb 4f states are situated ~ 6 eV below the Fermi level with a splitting of 0.7 eV between the $j = 5/2$ and $j = 7/2$ components. Pinned to the Fermi level appears the 14th f-state as a narrow peak, which is partially occupied. The Fe d states dominate the region between 3 eV below and 2 eV above the Fermi level, with hybridization with Ge p and Yb s and d states, in particular, at lower energies. The Ge s states dominate the split-off bands at 10–8 eV below the Fermi level.

4. SUMMARY AND CONCLUSIONS

The pressure-induced effective valence change of Yb ions in YbFe_2Ge_2 at room temperature has been measured with RXES and PFY techniques. The valence develops approximately linearly from an intermediate value of 2.72(2) at ambient pressure to close to trivalency at ~ 10 GPa (around QCP, $P_c = 9$ GPa). A few other Yb systems with the same ThCr_2Si_2 -type structure compare well with the valence changes observed in YbFe_2Ge_2 . In YbNi_2Ge_2 and YbPd_2Si_2 ,³⁹ pressure-induced Yb valence transitions associated with QCPs (near 6 and 1 GPa, respectively) were observed with smoothly varying Yb valence toward near trivalency at pressures above 10 GPa. In both cases the Yb valence varies less than $\Delta\nu = 0.01$, which is significantly less variation than observed in the present work for YbFe_2Ge_2 for the same pressure range. Interestingly, the effect of temperature on the effective Yb valence was also identified for YbNi_2Ge_2 and found of the same order, that is, $\nu = 2.86$ at 18 K and $\nu = 2.95$ at 300 K.⁴⁰ The valence transition seen in YbMn_2Ge_2 ¹⁷ with pressure and at room temperature is even more drastic, as the Yb valence increases by ~ 0.3 from ambient pressure to $P = 1.35$ GPa and only subsequently increases further at a similar pace to that of YbFe_2Ge_2 up to near trivalency above 15 GPa. Clearly, more detailed temperature investigations for both YbFe_2Ge_2 and YbMn_2Ge_2 would be highly desirable.

SIC-LSD calculations have been performed and show increasing effective valence of Yb with compression in YbFe_2Ge_2 , however, at a slower pace than measured and more similar to the pace measured for YbNi_2Ge_2 and YbPd_2Si_2 . The importance of Fe magnetism is confirmed by the calculations, which also show that the Fe spin moments are largely suppressed during compression in YbFe_2Ge_2 near the QCP. More detailed magnetic measurements like Mössbauer and neutron scattering are required to shed further light on the magnetic ordering in YbFe_2Ge_2 . On comparing the structural behavior of YbFe_2Ge_2 with YbMn_2Ge_2 ¹⁷ under high pressure conditions, a distinct difference is that a structural change to a monoclinic crystal phase occurs in YbMn_2Ge_2 above 30 GPa, while the current XRD results show that a pressure-induced structural change, if any, would occur only at pressures above 50 GPa for YbFe_2Ge_2 .

AUTHOR INFORMATION

Corresponding Author

*E-mail: ravhi@physics.unlv.edu.

Notes

The authors declare no competing financial interest.

ACKNOWLEDGMENTS

Work at the Univ. of Nevada Las Vegas (ALC) is funded by U.S. Department of Energy Award No. DE-SC0001928. Portions of this work were performed at HPCAT (Sector 16), Advanced PhotonSource (APS), Argonne National Laboratory. HPCAT operations are supported by DOE-NNSA under Award No. DE-NA0001974 and DOE-BES under Award No. DE-FG02-99ER45775, with partial instrumentation funding by NSF. The Advanced Photon Source is a U.S. Department of Energy (DOE) Office of Science User Facility operated for the DOE Office of Science by Argonne National Laboratory under Contract No. DE-AC02-06CH11357. Sample preparation at Los Alamos National Laboratory (LANL) was performed under the auspices of the

U.S. DOE, OBES, Division of Materials Sciences and Engineering.

REFERENCES

- (1) Stewart, G. R. *Rev. Mod. Phys.* **2001**, *73*, 797–855.
- (2) Si, Q.; Steglich, F. *Science* **2010**, *329*, 1161–1166.
- (3) Löhneysen, H. V.; Rosch, A.; Vojta, M.; Wölfle, P. *Rev. Mod. Phys.* **2007**, *79*, 1015–1075.
- (4) Holmes, A. T.; Jaccard, D.; Miyake, K. *J. Phys. Soc. Jpn.* **2007**, *76*, 051002.
- (5) Custers, J.; Gegenwart, P.; Wilhelm, H.; Neumaier, K.; Tokiwa, Y.; Trovarelli, O.; Geibel, C.; Steglich, F.; Pépin, C.; Coleman, P. *Nature (London, U. K.)* **2003**, *424*, 524–527.
- (6) Parthé, E.; Chabot, B. In *Handbook on the Physics and Chemistry of Rare Earths*; Gschneidner, K. A., Jr., Eyring, L., Eds.; Elsevier: Amsterdam, 1984; Vol. 6, Ch. 48, p 113.
- (7) Bara, J. J.; Hryniewicz, H. U.; Milos, A.; Szytula, A. *J. Less-Common Met.* **1990**, *161*, 185–192.
- (8) Larrea, J.; Fontes, M.; Baggio-Saitovitch, E.; Eichler, A.; Abd-Elmeguid, M. M.; Geibel, C.; Continentino, M. J. *J. Phys. Soc. Jpn.* **2007**, *76* (Suppl. A), 156–161.
- (9) Yamaoka, H.; Ikeda, Y.; Jarrige, I.; Tsujii, N.; Yamamoto, Y.; Mizuki, J.; Lin, J.-F.; Hiraoka, N.; Ishii, H.; Tsuei, K.-D.; Kobayashi, T. C.; Honda, F.; Onuki, Y.; Zekko, Y. *Phys. Rev. Lett.* **2014**, *113*, 086403.
- (10) Larrea, J.; Fontes, M. B.; Baggio-Saitovitch, E. M.; Plessel, J.; Abd-Elmeguid, M. M.; Ferstl, J.; Geibel, C.; Pereira, A.; Jornada, A.; Continentino, M. A. *Phys. Rev. B: Condens. Matter Mater. Phys.* **2006**, *74*, 140406.
- (11) Subedi, A. *Phys. Rev. B: Condens. Matter Mater. Phys.* **2014**, *89*.
- (12) Singh, D. J. *Phys. Rev. B: Condens. Matter Mater. Phys.* **2014**, *89*, 024505.
- (13) Ferstl, J.; Rosner, H.; Geibel, C. *Phys. B* **2006**, *378–380*, 744–745.
- (14) Fujiwara, T.; Aso, N.; Yamamoto, H.; Hedo, M.; Saiga, Y.; Nishi, M.; Uwatoko, Y.; Hirota, K. *J. Phys. Soc. Jpn.* **2007**, *76* (Suppl. A), 60–61.
- (15) Ran, S.; Bud'ko, S. L.; Canfield, P. C. *Philos. Mag.* **2011**, *91*, 4388–4400.
- (16) Zou, Y.; Feng, Z.; Logg, P. W.; Chen, J.; Lampronti, G.; Grosche, F. M. *Phys. Status Solidi RRL* **2014**, *8*, 928–930.
- (17) Kumar, R. S.; Svane, A.; Vaitheeswaran, G.; Zhang, Y.; Kanchana, V.; Hofmann, M.; Campbell, S. J.; Xiao, Y.; Chow, P.; Chen, C.; Zhao, Y.; Cornelius, A. L. *Inorg. Chem.* **2013**, *52*, 832–839.
- (18) Dallera, C.; Grioni, M.; Shukla, A.; Vanko, G.; Sarrao, J. L.; Rueff, J. P.; Cox, D. L. *Phys. Rev. Lett.* **2002**, *88*, 196403.
- (19) Dallera, C.; Annese, E.; Rueff, J. P.; Palenzona, A.; Vanko, G.; Braicovich, L.; Shukla, A.; Grioni, M. *Phys. Rev. B: Condens. Matter Mater. Phys.* **2003**, *68*, 245114.
- (20) Kumar, R. S.; Svane, A.; Vaitheeswaran, G.; Kanchana, V.; Bauer, E. D.; Hu, M.; Nicol, M. F.; Cornelius, A. L. *Phys. Rev. B: Condens. Matter Mater. Phys.* **2008**, *78*, 075117.
- (21) Perdew, J. P.; Zunger, A. *Phys. Rev. B: Condens. Matter Mater. Phys.* **1981**, *23*, 5048–5079.
- (22) Svane, A. *Phys. Rev. B: Condens. Matter Mater. Phys.* **1996**, *53*, 4275–4286.
- (23) Strange, P.; Svane, A.; Temmerman, W. M.; Szotek, Z.; Winter, H. *Nature (London, U. K.)* **1999**, *399*, 756–758.
- (24) Temmerman, W. M.; Petit, L.; Svane, A.; Szotek, Z.; Lüders, M.; Strange, P.; Staunton, J. B.; Hughes, I. D.; Györfy, B. L. In *Handbook on the Physics and Chemistry of Rare Earths*; Gschneidner, K. A., Jr., Bünzli, J. C. G., Pecharsky, V. K., Eds.; Elsevier: Amsterdam, 2009; Vol. 39, Ch. 241, p 1.
- (25) Temmerman, W. M.; Szotek, Z.; Svane, A.; Strange, P.; Winter, H.; Delin, A.; Johansson, B.; Eriksson, O.; Fast, L.; Wills, J. M. *Phys. Rev. Lett.* **1999**, *83*, 3900–3903.
- (26) Svane, A.; Temmerman, W. M.; Szotek, Z.; Petit, L.; Strange, P.; Winter, H. *Phys. Rev. B: Condens. Matter Mater. Phys.* **2000**, *62*, 13394–13399.
- (27) Svane, A.; Strange, P.; Temmerman, W. M.; Szotek, Z.; Winter, H.; Petit, L. *Phys. Status Solidi B* **2001**, *223*, 105–116.
- (28) Hammersley, A. P.; Svensson, S. O.; Hanfland, M.; Fitch, A. N.; Häusermann, D. *High Pressure Res.* **1996**, *14*, 235–248.
- (29) Howard, C. J.; Hunter, B. *International Union of Crystallography, Commission on Powder Diffraction -Newsletter* **1998**, *20*, 21 unpublished.
- (30) Varma, C. M. *Rev. Mod. Phys.* **1976**, *48*, 219–238.
- (31) Temmerman, W. M.; Svane, A.; Szotek, Z.; Winter, H.; Beiden, S. In *Electronic Structure and Physical Properties of Solids: The Uses of the LMTO Method*; Dreyssé, H., Ed.; Lecture Notes in Physics; Springer-Verlag: Berlin, 2000; Vol. 535, pp 286–312.
- (32) Andersen, O. K. *Phys. Rev. B* **1975**, *12*, 3060–3083.
- (33) Andersen, O. K.; Jepsen, O. *Phys. Rev. Lett.* **1984**, *53*, 2571–2574.
- (34) Birch, F. *Phys. Rev.* **1947**, *71*, 809–824.
- (35) Venturini, G.; Malaman, B. *J. Alloys Compd.* **1996**, *235*, 201–209.
- (36) Sengupta, K.; Hossain, Z.; Geibe, C.; Umeo, K.; Takabatake, T.; Forthaus, M.; Abd-Elmeguid, M. M. *Desy Annual Report* (http://hasyweb.desy.de/science/annual_reports/2007_report/part1/contrib/42/22100.pdf).
- (37) Plessel, J.; Abd-Elmeguid, M.; Sanchez, J.; Knebel, G.; Geibel, C.; Trovarelli, O.; Steglich, F. *Phys. Rev. B: Condens. Matter Mater. Phys.* **2003**, *67*, 180403.
- (38) Miyake, K. *J. Phys.: Condens. Matter* **2007**, *19*, 125201.
- (39) Yamaoka, H.; Jarrige, I.; Tsujii, N.; Lin, J.-F.; Hiraoka, N.; Ishii, H.; Tsuei, K.-D. *Phys. Rev. B: Condens. Matter Mater. Phys.* **2010**, *82*, 035111.